A polymer gel index-matched to water enables diverse applications in fluorescence microscopy

Xiaofei Han[1,2*,^], Yijun Su[1,3*,^], Hamilton White[4,5*,^], Kate M. O'Neill[6, 7], Nicole Y. Morgan[8], Ryan Christensen[1], Deepika Potarazu[1], Harshad D. Vishwasrao[3], Stephen Xu[1], Yilun Sun[9], Shar-yin Huang[9], Mark W. Moyle[10], Qionghai Dai[2], Yves Pommier[9], Edward Giniger[6], Dirk R. Albrecht[4,11, &], Roland Probst[12, &], Hari Shroff[1, 3, 13, &]

1. Laboratory of High Resolution Optical Imaging, National Institute of Biomedical Imaging and Bioengineering, National Institutes of Health, Bethesda, Maryland, USA
2. Department of Automation, Tsinghua University, 100084, Beijing, China
3. Advanced Imaging and Microscopy Resource, National Institutes of Health, Bethesda, Maryland, USA
4. Department of Biomedical Engineering, Worcester Polytechnic Institute, 100 Institute Road, Worcester, MA, 01609, USA
5. Department of Neurobiology, University of Massachusetts Medical School, Worcester, MA 01655, USA
6. National Institute of Neurological Disorders and Stroke, NIH, Bethesda, MD, 20892, USA.
7. Institute for Physical Science and Technology, University of Maryland College Park, College Park, Maryland, USA
8. National Institute of Biomedical Imaging and Bioengineering, National Institutes of Health, Bethesda, Maryland, USA
9. Developmental Therapeutics Branch and Laboratory of Molecular Pharmacology, Center for Cancer Research, National Institutes of Health, Bethesda, Maryland, USA
10. Department of Neuroscience and Department of Cell Biology, Yale University School of Medicine, New Haven, CT 06536, USA.
11. Department of Biology and Biotechnology, Worcester Polytechnic Institute, 100 Institute Road, Worcester, MA, 01609, USA.
12. ACUITYnano, Innovation in Biomedical Imaging, North Bethesda, Maryland, USA
13. Marine Biological Laboratory Fellows Program, Woods Hole, MA, USA

*Equal contribution
& Equal contribution
^ Correspondence to hxf16@mails.tsinghua.edu.cn, suy4nih@gmail.com, hawhite@wpi.edu

Abstract

We demonstrate diffraction-limited and super-resolution imaging through thick layers (tens-hundreds of microns) of BIO-133, a biocompatible, UV-curable, commercially available polymer with a refractive index (RI) matched to water. We show that cells can be directly grown on BIO-133 substrates without the need for surface passivation and use this capability to perform extended time-lapse volumetric imaging of cellular dynamics 1) at isotropic resolution using dual-view light-sheet microscopy, and 2) at super-resolution using instant structured

illumination microscopy. BIO-133 also enables immobilization of 1) *Drosophila* tissue, allowing us to track membrane puncta in pioneer neurons, and 2) *Caenorhabditis elegans*, which allows us to image and inspect fine neural structure and to track pan-neuronal calcium activity over hundreds of volumes. Finally, BIO-133 is compatible with other microfluidic materials, enabling optical and chemical perturbation of immobilized samples, as we demonstrate by performing drug and optogenetic stimulation on cells and *C. elegans*.

Introduction

Fluorescence microscopy spurs biological discovery, especially if imaging is performed at high spatiotemporal resolution and under physiologically relevant conditions. Coupling fluorescence microscopy with strategies for immobilizing or confining samples enables further applications, particularly when studying organisms that move rapidly. For example, the transparency and genetic accessibility[1] of the nematode *C. elegans* has made it an ideal system for studying the growth, morphology and function of individual cells in the context of the whole organism[2,3]**;** yet imaging the living animal without motion blur usually requires immobilization with chemical[4,5], steric[6,7], or microfluidic[8-11] means.

Microfluidic systems provide efficient immobilization and handling[12-18] for studying cellular morphology[19,20] and dynamics[21], neuronal function[22-24], behavior[25-27], and lifespan[28,29]. Hydrogels (either independently[7,30] or in conjunction with microfluidics[31]) have also been demonstrated as highly useful materials with tunable mechanical[32], diffusive, and optical properties[33] that are well-suited for long-term imaging applications[7,34,35].

Unfortunately, relatively few attempts have been made to index-match immobilization devices[36-39]. The high refractive index (RI, n) of materials commonly used in microfluidics, such as polydimethoxylsilane (PDMS), causes significant optical aberrations[40,41] due to the RI mismatch that occurs at the interface between the polymer (n_{PDMS} ~ 1.41) and an aqueous sample (n_{water} = 1.33). These aberrations severely degrade image focus, resolution, and signal, compromising the performance of immobilization devices by reducing the information content of the resulting data. Hydrogels offer a lower RI (n ranging from 1.34 – 1.41) depending on thickness and polymerization conditions[33]. Although the RI of these materials is better matched to living samples, even a small mismatch in RI causes a noticeable deterioration in image quality[42]. Image degradation is particularly obvious when using water-dipping lenses designed for imaging living samples, such as those employed in high-resolution light-sheet fluorescence microscopy (LSFM)[43-45].

Here we demonstrate a broadly applicable refractive-index-matched specimen mounting method that introduces negligible aberration when imaging living samples with high-resolution light-sheet microscopy and super-resolution microscopy. We show its utility in combination with microfluidics, enabling applications in high-resolution, volumetric imaging of cells, *Drosophila* tissue, and *C. elegans* adults and larvae. Our method takes advantage of the commercially available UV curable optical polymer BIO-133 (MY Polymers Ltd.) that has a refractive index matched to water (n = 1.333), is non-fluorescent, and is non-toxic. We show that 1) BIO-133 provides a gas permeable, inert, and biocompatible scaffold on which to grow and image tissue culture cells, 2) enables rapid tissue or animal encapsulation, and 3) is compatible with other microfluidic mounting schemes and optical or chemical perturbations.

Results

BIO-133 does not introduce additional optical aberrations

We assessed the optical properties of BIO-133 by using dual-view light-sheet microscopy (diSPIM[43,46]) to image 100 nm yellow-green beads placed under polymer layers of progressively increasing thickness (**Fig. 1, Methods**). In the most common diSPIM implementation, two identical 0.8 numerical aperture (NA) water-dipping objectives mounted above a planar substrate (usually a glass coverslip) alternately illuminate the sample with a light sheet and detect the resulting fluorescence. Since both illumination and detection planes are angled at ~45 degrees with respect to the glass coverslip, imaging through a polymer gel with surface parallel to the coverslip will introduce significant lateral ('x' direction, **Fig. 1a**) and axial ('z' direction, **Fig. 1a**) aberrations if the gel's refractive index differs from that of water.

As predicted, we observed this effect when imaging beads embedded under polymers with different RIs (**Fig. 1b, c**). Under no polymer, images of beads approximate the system point spread function, with measured lateral and axial full width at half maximum (FWHM) 395.9 +/- 7.7 nm and 1527.9 +/- 119.5 nm (*N* = 70 beads), respectively. Imaging beads under PDMS caused severe aberrations (**Fig. 1c**), more than doubling the lateral FWHM under a 25 μm layer (816.8 +/-24.9 nm) with progressive deterioration under thicker polymer layers (**Fig. 1b**). We also observed aberrations (**Fig. 1b, c**) under poly(ethylene-glycol) diacrylate (PEG-DA)[7] and fluorinated ethylene polymer (FEP)[47], albeit to lesser extent as the refractive indices of these polymers are closer to water. By contrast, beads imaged under BIO-133 showed negligible visual aberrations or measurable degradation in image quality (**Fig. 1b, c, Supplementary Table 1**), even under a 150 μm thick film, the largest thickness we tested (lateral FWHM 416.5 +/- 8.5 nm). We attribute this result to the refractive index of BIO-133, which we measured to be 1.333. We also verified, under 488 nm, 561 nm, and 637 nm illumination, that BIO-133 introduces negligible autofluorescence (**Supplementary Fig. 1**).

High- and super-resolution imaging of cells through a layer of BIO-133

BIO-133 has permeability to oxygen about 2-3 times greater than PDMS and has water repellent properties (Personal Communication, Ehud Shchori, My Polymers, Ltd.). These material properties are advantageous for maintaining physiologically relevant cell culture conditions. Thus, we investigated whether BIO-133 could provide an inert and biocompatible scaffold for single cell imaging (**Supplementary Table 2a**). After a curing and leaching treatment (**Methods**), U2OS cells seeded on a 50 μm layer of BIO-133 adhered and displayed similar morphology and growth rate to cells grown on glass coverslips (**Fig. 2a, Supplementary Fig. 2**). Similar results were obtained using HCT-116 (human colon carcinoma) cells that express endogenous topoisomerase I-GFP, and we also observed similar expression and localization of tagged proteins compared to cells cultured on glass coverslips **(Supplementary Figs. 2, 3)**.

To demonstrate that transfected cells seeded directly on BIO-133 could be imaged at high spatiotemporal resolution, we created BIO-133 substrates on PDMS supports (**Supplementary Fig. 4**) and imaged cells expressing mEmerald-Tomm20, a fluorescent marker

132 of the outer mitochondrial membrane, through a 50 μm thick BIO-133 layer using diSPIM (**Fig.**
133 **2b, c**). The jointly registered and deconvolved data acquired from two views displayed isotropic
134 spatial resolution (**Fig. 2c, d**), allowing us to clearly visualize individual mitochondria and their
135 dynamics (**Supplementary Video 1**), including mitochondrial fusion and fission (**Fig. 2d**). We
136 also used BIO-133 in conjunction with diSPIM to construct a simple gravity-driven flow
137 cytometry setup, obtaining clear images of DAPI stained nuclei as they flowed through the
138 chamber (**Supplementary Fig. 5, 6, Supplementary Video 2**).
139 Next, we sought to image subcellular targets at spatial resolution beyond the diffraction
140 limit, so we turned to instant structured illumination microscopy (iSIM)[48], which enables high-
141 speed super-resolution imaging. We again seeded U2OS cells expressing mEmerald-Tomm20 on
142 a 50 μm BIO-133 film, this time imaging them with iSIM using a water dipping lens in an
143 inverted geometry (**Fig. 2e**). Again, BIO-133 provided aberration-free imaging, enabling us to
144 visualize the internal mitochondrial space absent Tomm20 (**Fig. 2f, g, Supplementary Video 3**).
145 We also visualized LAMP-1-GFP-stained lysosome dynamics in wild type HCT-116 cells grown on
146 another BIO-133 film of 50 μm thickness (**Supplementary Fig. 7, Supplementary Video 4**). As a
147 third example, we grew multiple layers of HCT-116 cells on BIO-133, and immunostained the
148 cells for lamin A/C, Tomm20, and actin (**Fig. 2h**), obtaining clear images of these structures
149 through the volume of the sample (**Fig. 2i, Supplementary Video 5**). We conclude that BIO-133
150 is compatible with multicolor, super-resolution imaging in live and fixed targets.
151
152 *BIO-133 enables subcellular imaging, segmentation, and tracking within immobilized living*
153 *tissue*
154
155 In addition to monitoring the dynamics of organelles within single cells, we also
156 immobilized and imaged multicellular structures in flies and worms at high spatiotemporal
157 resolution, using diSPIM in conjunction with BIO-133 for sample immobilization (**Fig. 3,**
158 **Supplementary Table 2b**). The developing *Drosophila* wing has long been a model for axon
159 growth and neuronal pathfinding and differentiation[49,50]. More recently, spinning disk confocal
160 microscopy was used to dissect the role of cytoskeletal organization and dynamics in shaping
161 the morphogenesis and growth of the TSM1 pioneer sensory neuron axon in explanted early-
162 pupal wing imaginal discs[51,52]. In those experiments, phototoxicity and photobleaching limited
163 imaging duration to ~30 volumes, with image volumes acquired every 3 minutes. Wings were
164 sandwiched between two glass coverslips to immobilize the preparation and prevent it from
165 moving during imaging, but this scheme introduces unacceptable aberrations if imaging with
166 the less phototoxic diSPIM. Instead, we immobilized wings with a thin layer of BIO-133 (**Fig. 3a,**
167 **Supplementary Fig. 8**), which enabled sustained volumetric imaging with diSPIM. We acquired
168 360 single-view volumes (5 s inter-volume interval, spanning 30 minutes) of tdTomato-CD4
169 expressed in TSM1 and the neighboring L3 neuron, marking neuronal membranes (**Fig. 3b**). In
170 addition to observing slower remodeling of the TSM1 growth cone (**Fig. 3c, top**) our imaging
171 rate also enabled us to capture rapid movement of membrane-labeled puncta that appeared to
172 traffic along the L3 axon shaft (**Fig. 3c, bottom, Supplementary Video 6**). Puncta were also
173 evident in comparative spinning disk confocal datasets (**Supplementary Fig. 9**).
174 In another example, we used soft lithography techniques[53] to cast BIO-133 into
175 microfluidic devices suitable for trapping *C. elegans* (**Supplementary Fig. 10**). Introducing adult

176 worms into the channels via suction **(Fig. 3a**), we imaged fine structures (**Fig. 3d**) and functional
177 activity **(Fig. 3e-j**) in living animals at isotropic resolution. Animals were sufficiently immobile
178 that we could serially acquire and fuse the two diSPIM views[54] to obtain reconstructions free of
179 motion blur. In strains expressing GFP sparsely targeted to a few neurons, we resolved axons
180 and dendrites (likely from amphid neurons, **Fig. 3d**) within anesthetized *C. elegans*. When
181 imaging the genetically encoded calcium indicator GCaMP6s[55] and mCherry targeted pan-
182 neuronally[56] in immobilized adult animals without anesthetic, our volume imaging rate of 1.25
183 Hz (simultaneous acquisition of red and green channels) enabled us to segment and track 126
184 nuclei in the animal head (**Fig. 3e,f Supplementary Video 7**), permitting inspection of
185 spontaneously active nuclei (**Fig. 3f, g**) over our 450 volume (6 minute) experiment. Intriguingly,
186 we observed a pair of nuclei (#79 and #15, **Fig. 3e, g**) that exhibited in-phase, rhythmic activity
187 with slow (45-80 s) period (**Supplementary Video 7**), as well as nuclei showing out-of-phase
188 activity with respect to this pair (#27). In another experiment, we simply embedded *C. elegans*
189 larvae expressing the same pan-nuclear GCaMP6s marker in a cured disk of BIO-133 (**Fig. 3a**),
190 recording volumes from one side to obtain volumes at 4 Hz, for 250 volumes. Despite the
191 poorer axial resolution of single-sided imaging, and the smaller size of the larval nuclei, we were
192 able to again segment and track 110 nuclei in the head of the animal, identifying calcium
193 transients in spontaneously active nuclei with a time resolution of 0.25 s (**Fig. 3h-j,**
194 **Supplementary Video 8**).
195 The droplet-based design also enabled easy recovery of animals post-imaging. 26 / 28
196 animals were recovered even ~12 hours after embedding, confirming our suspicion that cured
197 BIO-133 is inert, gas permeable, water repellant, and does not obviously affect animal viability
198 (the remaining two animals died within the BIO-133 capsule due to internal hatching of
199 embryos within the animals). The water repellency of BIO-133 likely contributes to retaining the
200 animal's intrinsic hydration and thus viability during encapsulation. The ease at which *C.*
201 *elegans* can be immobilized and imaged at high spatiotemporal resolution suggests useful
202 synergy with multicolor strategies that permit unambiguous neural identification[23].
203
204 *BIO-133 is compatible with chemical and optogenetic perturbations*
205
206 The ability to specifically perturb and subsequently follow biological processes by
207 observing morphological or functional changes is valuable in dissecting biological processes.
208 We conducted several studies to show that BIO-133-mounted samples are compatible with
209 such perturbations (**Fig. 4**). First, we conducted a simple drug assay by modifying our BIO-
210 133/PDMS cellular scaffolds (**Fig. 2b, Supplementary Fig. 11**) so that U2OS cells could be
211 exposed (**Fig. 4a**) to carbonyl cyanide m-chlorophenyl hydrazine (CCCP), an inhibitor of
212 oxidative phosphorylation. Because we could clearly observe cells through the BIO-133 layer
213 using diSPIM, we observed that, compared to control cells in a neighboring well (**Fig. 4a-c**),
214 within minutes of exposure the treated cells showed mitochondrial fragmentation, eventually
215 exhibiting major disruption to the mitochondrial network (**Fig. 4b, c, Supplementary Video 9**).
216 Chemically stimulating animals directly embedded in BIO-133 is difficult, since BIO-133 is
217 not permeable to aqueous solutions. One solution is to introduce chemicals via microfluidic
218 channels (such as those shown in **Fig. 3d-g**). Alternatively, we explored using PEG-DA for
219 immobilization and aqueous permeability, above a microfluidic layer for stimulus introduction

220 and control, and beneath a BIO-133 layer to enclose the fluidic path. Using a thin PEG-DA disk
221 allows easy transfer of different embedded organisms on the same imaging setup, and
222 repeated imaging of the same animals over many hours if desired. We constructed a hybrid
223 multi-material device composed of a PDMS microfluidic base bonded to a BIO-133 upper
224 membrane that sealed in a small PEG-DA disk containing tens of embedded nematodes[7]
225 (**Supplementary Fig. 12, Fig. 4a**). Chemicals applied via flow channels diffuse into the PEG-DA
226 disk, evoking neural responses that can be imaged through the BIO-133 viewing layer with
227 widefield microscopy or diSPIM (**Fig. 4d-g, Methods**). We embedded 15 animals expressing
228 GCaMP2.2b in AWA chemosensory neurons[57] in a PEG-DA disk and applied 1.1 μM diacetyl
229 pulses, which directly activate these neurons via the ODR-10 chemoreceptor[57,58]. Using
230 widefield microscopy, we recorded robust calcium transients from all animals and observed a
231 characteristic sensory adaptation to repeated stimulation (**Fig. 4e**). The initiation of sensory
232 neural responses varied slightly due to diffusion of diacetyl stimulus through the PEG-DA disk to
233 animals embedded in different planes (**Supplementary Fig. 13**). Next, we examined individual
234 neuron responses by using the same apparatus with diSPIM (**Fig. 4f,g Supplementary Video**
235 **10**). Our imaging provided sufficient spatial resolution to distinguish subcellular responses,
236 observing faster on and off dynamics of fluorescent transients in the dendrites than in the
237 soma[59].
238 Other stimulation modalities (such as light, temperature, and mechanical vibration) are
239 directly transmissible through BIO-133, and these can be applied directly to cells and organisms
240 embedded in the polymer in a simpler preparation. Optogenetic neural activation is a
241 particularly advantageous tool, allowing remote light-induced activation or suppression of
242 neurons. We embedded nematodes expressing the red light activated cation channel
243 Chrimson[60] and GCaMP2.2b[7] directly in BIO-133 disks and monitored calcium readout with
244 diSPIM during repeated red light stimulation pulses (**Fig. 4a,h,i, Supplementary Video 11**). We
245 observed increases in fluorescence after each stimulus (**Fig. 4h**), and again could clearly localize
246 such transients to subcellular areas including soma, dendrite, and axon (**Fig. 4i**).
247
248 **Discussion**
249
250 BIO-133 is commercially available, rapidly curing, gas permeable, inert, water repellent,
251 and biocompatible. It is not autofluorescent under visible illumination and does not introduce
252 additional aberration when imaging with water-dipping or water-immersion objective lenses
253 designed for aqueous specimens. These characteristics make it well-suited to microfluidic
254 experiments under physiological conditions, particularly with the many LSFM systems that use
255 such lenses. We suspect that capillary mounting[47], often used for mounting zebrafish in LSFM,
256 could be improved if BIO-133 were used instead of the FEP material commonly used in this
257 application. Our finding that cells can be directly grown on BIO-133 without additional surface
258 treatment may prove useful in non-standard LSFM geometries that previously employed RI-
259 matched materials with passivated surfaces[45], or in ultra-high-throughput light-sheet
260 imaging[61,62].
261 We also found that BIO-133 does not noticeably degrade imaging performed in more
262 traditional inverted microscope geometries, including in super-resolution imaging. This
263 capability suggests that using BIO-133 could improve imaging in studies of cell morphology,

mechanics, migration, and motility, e.g., when using micropillars[20,63] or in traction force microscopy[64].

We bonded BIO-133 to glass and PDMS with silicone-based adhesive tape, or reversibly to glass via van der Waals forces. The elastic modulus of cured BIO-133 (5 MPa) is similar to that of PDMS (3.7 MPa). Thus, similar to PDMS[65], BIO-133 conforms to minor imperfections in glass and bonds to it by weak van der Waal forces, creating a reversible bond and a watertight seal. We suspect further tuning of adhesive, optical and mechanical properties of this intriguing polymer is possible but will depend on knowing the chemical formula, which is currently proprietary.

Author Contributions

Conceived project: R.P., H.S. Designed experiments: X.H., Y.S., H.W., K.M.O., H.D.V., E.G., D.A., R.P., H.S. Provided technical advice and resources for microfluidics: N.M., R.P., H.W., D.A. Provided biological advice: R.C., Y.S., S.H., Y.P. Created new reagents: S.H., Y.P, M.W.M. Performed experiments: X.H., Y.S., H.W., K.M.O., D.P., H.D.V., R.P. Tracked nuclei in GCaMP imaging experiments: X.H., Y.S., S.X. Wrote paper with input from all authors: X.H., Y.S., H.W., D.A., R.P., H.S. Supervised research: Q.D., Y.P., E.G., D.A., R.P., H.S. Directed research: H.S.

Acknowledgements

This research was funded in part by the National Institute of Biomedical Imaging and Bioengineering, the National Institute of Neurological Disorders and Stroke, and the Center for Cancer Research of the National Cancer Institute within the National Institutes of Health (Z01 BC 006161), and the National Science Foundation (CBET 1605679). We thank George Patterson for the use of his cell culture facilities, Leighton Duncan and Daniel Colón-Ramos for kindly providing strains and for conducting initial pilot experiments and their careful read, Evan Ardiel and Eviatar Yemini for providing helpful feedback on pan-nuclear GCaMP recordings, Ron Zohar and Ehud Shchori for providing useful information on BIO-133, and Hank Eden for providing helpful feedback on the manuscript. K.M.O. and E.G. were supported by NINDS Z01-NS003013 to E.G. K.M.O. was also jointly supported by AFOSR grant number FA9550-16-1-0052 to W. Losert at UMD College Park. M.W.M was supported by NIH grant F32-NS098616.

Disclaimer: The NIH, its officers, and staff do not recommend or endorse any company, product, or service.

Methods

Sample preparation

U2OS, wild type (WT) HCT-116, and HCT-116 TOP1-GFP cell culture

U2OS (ATCC, HTB-96), WT HCT-116 (ATCC, CCL-247), and HCT-116 TOP1-GFP (see below) cells were cultured in DMEM (Lonza, 12-604F) media with 10% Fetal Bovine Serum at 37°C and 5% CO_2.

To tag the genomic topoisomerase I (TOP1) in WT HCT-116 cells, sequence CCTCACTTGCCCTCGTGCCT targeting a CRISPR site 77nt after the stop codon of TOP1 was cloned into pX330. Homology arms (of ~1 kb) upstream and downstream of the target site were cloned to flank a blasticidin - resistance gene, where the upstream homology arm was modified to replace the stop codon with a GFP domain connected to the protein-coding region of the last exon of TOP1 via a short poly-lysine linker. Both constructs were co-transfected into WT-HCT116 cell, followed by selection with 5 μg/mL of blasticidin 48 hours post transfection. GFP-positive cells were further selected by FACS.

Transfection of cells

Cells were cultured to 50% confluency and transfected using xTreme Gene HP DNA Transfection Reagent (Sigma, 6366236001). The transfection mixture contained 100 μL 1X PBS, 2 μL Transfection Reagent, and 200-1000 ng plasmid DNA. Cells were imaged 24-48 hours after transfection.

C. elegans samples

Nematode strains were grown on NGM plates seeded with OP50 bacteria. *C. elegans* imaged as young adults were synchronized by picking L4 stage worms 24 hours prior to the experiment and transferring them to seeded plates, and *C. elegans* imaged as larvae were directly picked from plates. Strain DCR6268 (*olaEx3632[pttx-3b::SL2::Pleckstrin homology domain::GFP::unc-54 3'UTR + pelt-7::mCh::NLS::unc-54 3'UTR]*) was used for imaging axons and dendrites (**Fig. 3d**). olaEx3632 was made by injecting plasmid DACR2285 (pttx-3b::SL2::Pleckstrin homology domain::GFP::unc-54 3'UTR) at 25 ng/uL and DACR2436 (pelt-7::mCh::NLS::unc-54 3'UTR) at 10 ng/μL. Strain AML32[56] (*wtfIs5 [rab-3p::NLS::GCaMP6s + rab-3p::NLS::tagRFP]*) was used for pan-nuclear neuronal calcium imaging (**Fig. 3e-j**); strain NZ1091(*kyIs587 [gpa-6p::GCaMP2.2b; unc-122p::dsRed]; kyIs5662 [odr-7p::Chrimson:SL2:mCherry; elt-2p::mCherry]*[7]) was used for chemical (**Fig. 4d-g**) and optogenetic stimulation (**Fig. 4h, i**) . For optogenetic stimulation, L4 stage animals were transferred to agar plates seeded with 62.5 μM all trans-retinal (ATR, Sigma Aldrich, R2500) for over 12 hours.

Drosophila samples

Drosophila stocks were obtained from the Bloomington *Drosophila* Stock Center: *neur-GAL4* (BL6393) and *UAS-CD4-td-Tomato* (BL35837). White prepupae were selected and aged for 13-14 h at 18°C followed by 1 h at 25°C (equivalent to 7.5–8 h at 25°C). These aged pupae were dissected in fresh culture media (CM; Schneider's Drosophila media + 10% fetal bovine serum, both from Life Technologies), and wing discs were isolated from the aged pupae and stored in fresh CM prior to mounting with BIO-133.

Characterizing the optical properties of polymers

Characterization of aberrations by visualizing fluorescent beads under different polymer layers

351 100 nm diameter yellow-green fluorescent beads (Invitrogen, F8803, 1:10000 dilution in water)
352 were coated on #1.5 coverslips (24 mm x 50 mm, VWR, 48393-241) coated with 0.1% w/v poly-
353 L-lysine (Sigma, P8920-100ML). We placed spacers (Precision Brand, 44910) of variable
354 thickness on one of the coverslips and deposited droplets of BIO-133, 10% PEG-DA (ESIBIO,
355 GS705) or UV-curable PDMS (Shin-Etsu Chemical, KER-4690) on the beads. The droplet was
356 then covered with another coverslip coated with beads and compressed with an iron ring. BIO-
357 133 and PEG-DA hydrogels were crosslinked at 312 nm (Spectroline ENB-280C) for 2 minutes.
358 PDMS was crosslinked at 312 nm for 5 minutes and post-cured at room temperature for one
359 day. Once cured, we separated the two cover glasses and kept the one with polymer/hydrogel
360 on it. For imaging through FEP films of different thickness (CS Hyde, 23-1FEP-24, 25 μm; 23-
361 2FEP-24, 50 μm; 23-3FEP-24, 75 μm; 23-5FEP-24, 125 μm), we immersed beads in 1μL water
362 and covered the sample with the FEP film. All bead images were acquired with a symmetric
363 0.8/0.8 NA diSPIM[43].
364
365 *Measurement of refractive index of polymers*
366 A refractometer (American Optical) was used to measure the refractive index of pure water,
367 BIO-133 film (My Polymer, BIO-133, 25 μm), PDMS film (Shin-Etsu Chemical, KER-4690, 25 μm),
368 FEP film (CS Hyde, 23-1FEP-24, 25 μm), and 10% PEG-DA hydrogel (100 μm). The refractive
369 index for each material was measured 3 times and the average value reported in **Fig. 1**.
370
371 *Measurement of BIO-133 autofluorescence*
372 A 50 μm thick BIO-133 film was deposited on a glass bottom dish (MatTek, P35G-1.5-14-C).
373 Images were acquired both on the BIO-133 area and an area without BIO-133, using an instant
374 structured illumination microscope (iSIM[48]) with 40 ms exposure time and 45 mW 488 nm
375 excitation, 70 mW 561 nm excitation, or 90 mW 639 nm excitation (measured with a power
376 meter immediately prior to the objective). Care was taken to ensure the illumination was
377 focused within the BIO-133 film. The two images were subtracted to measure the
378 autofluorescence of BIO-133 relative to glass (**Supplementary Fig. 1**).
379
380 **Cell growth and imaging using BIO-133 substrates**
381
382 *Fabrication of BIO-133 cell culture wells for diSPIM experiments*
383 BIO-133-sided PDMS substrates with 2.5 mm diameter wells (**Supplementary Fig. 4**) were used
384 for live cell imaging experiments (**Fig. 2b-d**). To make the BIO-133 bottom, a BIO-133 droplet
385 was positioned on a #1.5 glass coverslip (24 mm x 50 mm, VWR 48393-241) between two 50
386 μm plastic spacers (Precision Brand, 44910), covered with another coverslip , compressed with
387 a glass slide (Ted Pella, 260386) and cured with a UV lamp (365nm, Spectroline ENB-280C) for
388 15 minutes. After curing, the BIO-133 film was peeled off and exposed to UV light for another 2
389 hours in 70% ethanol. To make the PDMS well, 15 mL PDMS (Dow Inc. Sylgard 184) was poured
390 into a 10 cm plastic dish (Kord-Valmark, 2910) and cured for 2 hours at 80 °C to obtain a 2 mm
391 thick PDMS slab. We punched 2.5 mm diameter matching holes on the PDMS slab and a piece
392 of double-sided tape (Adhesives Research, ARCare 90880) using a 2.5 mm diameter circular
393 punch (Acuderm Inc., P2550). The PDMS slab and the tape were then cut into smaller pieces (~5

394 mm on a side) with a razor blade (Sparco, 01485). BIO-133 membranes, PDMS chunks and
395 double-sided tape were further disinfected in 70% ethanol for 2 hours. After disinfection, the
396 BIO-133 membrane was adhered to PDMS using the adhesive tape, so that the matching holes
397 became wells for cell culture. After seeding and growing cells in wells, the assembly was flipped
398 over for diSPIM imaging.
399
400 *Quantification of cell growth*
401 Cured and leached 50 μm thick BIO-133 films were deposited on glass bottom dishes (MatTek,
402 P35G-1.5-14-C). Similar aliquots of U2OS (or HCT 116 TOP1-GFP) cells were seeded onto BIO-
403 133 films or on another glass bottom dish without BIO-133 (MatTek, P35G-1.5-14-C). Dishes
404 seeded with cells were maintained between imaging experiments in an incubator at 37°C, 5%
405 CO_2. On each dish, a small area was selected and imaged using a widefield microscope equipped
406 with a 10x/0.25 NA objective lens each day, for three days. Cells numbers were estimated from
407 images with the Cell Counter ImageJ plugin (https://imagej.nih.gov/ij/plugins/cell-
408 counter.html). Each experiment was repeated three times. Raw images were divided by
409 Gaussian-blurred versions of themselves (sigma = 5 pixels) to flat-field images prior to display
410 (**Fig. 2a, Supplementary Fig. 2**).
411
412 *Live cell imaging through BIO-133 with diSPIM*
413 U2OS cells were cultured and transfected with 100-200 ng of mEmerald-Tomm20 plasmid
414 (Addgene, 54281) directly on the BIO-133 bottomed well plate. The well plate was inverted and
415 immersed in live cell imaging solution (Invitrogen, A14291DJ). Cells were imaged with a
416 symmetric 0.8/0.8 NA diSPIM, through the BIO-133 layer. 50 volumes were acquired with 3 s
417 intervals between dual-view volumes. Dual-view data were jointly deconvolved with ImageJ
418 plugin DiSPIM Fusion[54], and were drift- (with ImageJ plugin Correct 3D Drift
419 (https://imagej.net/Correct_3D_Drift) and bleach- corrected (with ImageJ function Bleach
420 Correction (https://imagej.net/Bleach_Correction, exponential fitting method) prior to display.
421
422 *Super-resolution imaging through BIO-133 with iSIM*
423 U2OS or WT HCT-116 cells were cultured and transfected with mEmerald-Tomm20 or LAMP1-
424 EGFP (Taraska Lab, NHLBI) on a 50 μm thick BIO-133 film. The BIO-133 film was cured on a glass
425 bottom dish (MatTek, P35G-1.5-14-C). A 60X, NA = 1.2 water objective (Olympus, PSF grade),
426 correction collar adjusted to 0.17, was used to image the cells through the glass and BIO-133
427 film using our home built iSIM system[48] and 488 nm excitation. Volumes were acquired every 3
428 s for U2OS cells expressing mEmerald-Tomm20 and every 7 s for WT HCT-116 cells expressing
429 LAMP1-EGFP. We used an exposure time of 80 ms, and a z-step of 0.25 μm for U2OS cells and
430 0.5 μm for WT HCT-116 cells. Live HCT-116 TOP1-GFP cultured on a 50 μm thick BIO-133 film or
431 on a glass bottom dish were imaged to acquire volumes with a step size of 0.5 μm. Raw images
432 were deconvolved with the Richardson-Lucy algorithm for 20 iterations, destriped in Fourier
433 space to remove striping artifacts[66], and bleach corrected
434 (https://imagej.net/Bleach_Correction). A median filter with kernel size 0.5 pixel was applied to
435 denoise mEmerald-Tomm20 and GFP-LAMP1 images prior to display.
436
437 *Immunolabeling and imaging of multilayered WT HCT-116 cells on BIO-133*

438 WT HCT-116 cells were cultured on a 50 μm thick BIO-133 film on a glass bottom dish until a
439 thick layer was visible by eye. Cells were fixed with 4% paraformaldehyde (Electron Microscopy
440 Sciences) in 1X PBS for 30 minutes at room temperature (RT). Cells were rinsed 3 times in 1X
441 PBS and permeabilized with 0.1% Triton X-100/PBS (Sigma, 93443) for 15 min at RT.
442 Permeabilized cells were rinsed 3 times with 1X PBS and incubated in 1X PBS with primary
443 antibody Rabbit-α-Tomm20 (Abcam, ab186735) and Mouse-α-LaminA/C (Abcam, ab244577) at
444 a concentration of 1:100 for 1 hour at RT. After primary antibody staining, cells were washed in
445 1X PBS for 5 min, three times. Cells were stained in 1X PBS with secondary antibody Donkey-α-
446 Rabbit Alexa Fluor 488 (Jackson Immuno Research, 711-547-003), Donkey-α-Mouse JF549
447 (Novusbio, NBP1-75119JF549) and Alexa Fluor 647 Phalloidin (Thermofisher, A22287) at a
448 concentration of 1:100 for 1 hour at RT. Cells were washed in 0.1% Triton X-100/PBS for 5 min,
449 three times. In each spectral channel, 46 slices were acquired on iSIM with an exposure time of
450 100 ms and a z-step of 0.5 μm. Raw images were deconvolved with the Richardson-Lucy
451 algorithm for 20 iterations and destriped in Fourier space to remove striping artifacts[66]. The 633
452 nm channel (Alexa Fluor 647 Phalloidin) was bleach corrected
453 (https://imagej.net/Bleach_Correction) across the z stack to compensate for decreased signal
454 further into the stack.
455
456 *Flow cytometry preparation*
457 Sample handling channels, 1 mm wide and 70 μm high, were formed by pouring 20 mL PDMS
458 (Dow Corning, Sylgard 184) on a positive mold made of packaging tape (Duck Brand) cut to the
459 desired dimensions with a craft cutter (Silhouette Cameo) and stuck in a 10 cm Petri dish. A thin
460 PDMS membrane (~0.5 mm) was air plasma (Harrick Plasma, PDC-32G (115V)) bonded to the
461 channel surface. Holes at the endpoints of the channel were created by punching the PDMS
462 membrane with a 1 mm diameter circular punch (Acuderm Inc., P150) after plasma treatment.
463 A 400 μm wide (142 μm height) imaging channel was cut directly from double-sided silicon-
464 based adhesive tape (Adhesives Research, ARCare 90880) with a craft cutter and stuck to the
465 PDMS device, thus creating a connection between the two sample handling channels in the
466 lower layer. A thin BIO-133 membrane (50 μm) was placed on top of the tape to seal the
467 channel. Two thick PDMS pieces with holes (6 mm and 2 mm diameter) were cut and air plasma
468 bonded to the device to provide fluidic access. When imaging, cells were added to the 6 mm
469 diameter reservoir, and output tubing (Dow Corning, 508-004) was connected to the 2 mm
470 hole. Flow speed was adjusted by changing the height of the output tubing. See also
471 **Supplementary Fig. 5.**
472
473 *Flow cytometry imaging of fixed, DAPI-stained U2OS cells*
474 U2OS cells were fixed in 4% Paraformaldehyde/PBS and subsequently stained with DAPI in 0.1%
475 Triton X-100/PBS (Sigma, 93443). The flow device was mounted on a 10 cm petri dish for
476 imaging with diSPIM. Fixed cells were added to the input port, producing steady flow through
477 the channel after several minutes. 1000 frames of the same image plane were acquired with
478 diSPIM at 50 frames per second under 'fixed sheet mode'.
479
480 **Live animal/tissue imaging through BIO-133 with diSPIM**
481

482 *Live imaging of BIO-133 embedded Drosophila wings*
483 A 13 μm thick BIO-133 film was created and cut into two rectangular pieces (4.5 mm x 10 mm)
484 and a square piece (10 mm x 10 mm). The rectangular pieces were deposited on a 10 cm petri
485 dish to form a 1 mm wide open-top channel. Early pupal fly wings were deposited into the
486 channel (convex side up) with 20-40 μL culture media, the square BIO-133 piece placed on top
487 to close the channel and additional culture media was carefully added to the dish (**Fig. 3a,**
488 **Supplementary Fig. 8)**. Single-view diSPIM imaging was then performed. 360 volumes were
489 acquired with 5 s inter-volume spacing, over 30 minutes. Volumes were deconvolved with
490 MATLAB and bleach corrected with ImageJ (https://imagej.net/Bleach_Correction, exponential
491 fitting method).
492
493 *Fabrication of microfluidics for C. elegans immobilization*
494 Standard soft lithography techniques[67] were used to fabricate an SU-8 (Kayaku Advanced
495 Materials, formerly Microchem Corp.) master mold for sets of four microfluidic funnels for
496 worm confinement as described[53]. To fabricate devices in BIO-133 (MY Polymers Ltd.), we
497 placed two spacers (100 μm, Precision Brand 44910) beside the pattern, poured polymer onto
498 the mold, covered the mold with a glass slide and cured the polymer under a UV lamp (365nm,
499 Spectroline ENB-280C) for 2 minutes. After curing, we peeled the BIO-133 off the mold,
500 punched inlet and outlet holes with a 1 mm diameter circular punch (Acuderm Inc., P150), and
501 sealed the device to a #1.5 cover glass (24 mm x 50 mm, VWR 48393-241) with double-sided
502 silicone-based adhesive tape (Adhesives Research, ARCare 90880). We cut out an aperture from
503 a 10 cm petri dish and used UV-curable optical cement (Norland Products Inc., Norland Optical
504 Adhesive NOA 68) to secure the coverslip carrying the microfluidic device over the aperture in
505 the petri dish. Inlet and outlet tubing (Dow Corning, 508-004) was clamped to the assembly
506 using a pair of hollow magnets (K&J Magnetics, R211-N52) placed above and below the
507 coverslip, as described[68]. Optical cement was again used to secure tubing to the magnets. See
508 also **Supplementary Fig. 10**.
509
510 *Live imaging of C. elegans through BIO-133 chambers*
511 To load worms into the immobilization device, we added a drop of M9 buffer containing worms
512 to the inlet and created vacuum at the outlet using a syringe. Within several minutes (for a 4-
513 channel chip), worms were observed to align in the channels. The petri dish was then filled with
514 water and worms were imaged with symmetric 0.8/0.8 NA diSPIM. For structural imaging, we
515 added 0.25 mM levamisole to the buffer to stop residual worm motion. For calcium imaging,
516 the outlet was connected to a peristaltic pump (Dolomite Microfluidics, 3200243) which
517 provided negative pressure to immobilize worms without using anesthetics. We simultaneously
518 imaged nuclei structure (TagRFP) and the nuclear-localized calcium response (GCaMP) with 488
519 nm and 561 nm excitation (Coherent) and image splitting devices on the detection side
520 (Hamamatsu W-VIEW GEMINI), using a previously described fiber-coupled diSPIM system[46].
521 Dual-view stacks were acquired every 0.8 s over 500 time points. Dual-color, dual-view images
522 were deconvolved and registered with ImageJ plugin DiSPIM Fusion[54].
523
524 *Droplet-based immobilization of nematodes prior to imaging, and recovery after imaging*

525 *C. elegans* were directly transferred from agar plates into a drop (~10 μL) of BIO-133 or 10%
526 PEG-DA (ESIBIO GS705) on a #1.5 cover glass (24 mm x 50 mm, VWR, 48393-241). The droplet
527 was positioned between two 100 μm spacers (Precision Brand, 44910), and was compressed by
528 a glass slide followed by 2-minute polymerization under a UV lamp (365nm, Spectroline ENB-
529 280C). After polymerization, worms were immobilized in the resulting gel disk. The gel disk was
530 then placed in a 10 cm petri dish or a standard chamber for diSPIM imaging. Single-view stacks
531 were acquired every 0.25 s for 250 time points. After imaging, worms could be released and
532 checked for viability by gently breaking the droplet with forceps. In some experiments, we
533 immersed the disks in M9 buffer for up to 12 hours, finding that live worms could also be
534 recovered after this period.
535
536 *Tracking nuclei, calcium imaging analysis*
537 TagRFP volumes were imported into Imaris and neurons tracked with Imaris for Tracking
538 (https://imaris.oxinst.com/products/imaris-for-tracking) to obtain the center of each neuron at
539 every timepoint. A custom MATLAB script was used to extract the calcium signal. For every
540 neuron, the average intensity of TagRFP channel I_{561} and the intensity of GCaMP channel I_{488}
541 were computed by averaging pixels within a 2 μm (adult) or 1.5 μm (larval) diameter sphere
542 placed around each center position. I_{561} and I_{488} were calculated from dual-view deconvolved
543 images (Fig. 3 f, g) or single-view raw data (Fig. 3 i, j). The ratio $R=I_{488}/I_{561}$ was used to minimize
544 non-GCaMP fluctuations. Neuronal activity for the datasets in **Fig. 3** was reported as $dR/R = (R -$
545 $R_0)/R_0$, where R_0 is the baseline for an individual neuron defined as its lower 20th percentile
546 intensity value.
547
548 **Chemical and optical perturbations in BIO-133 based imaging devices**
549
550 *Fabrication of chemical delivery devices for cells*
551 A modified PDMS well plate design (**Supplementary Fig. 11**) was applied to deliver chemical
552 perturbations to cells (**Fig. 4a-c**). A 400 μm thick BIO-133 film was created using the method
553 described above. 10 mL PDMS was cured in a 10 cm dish, PDMS tubing (Dow Corning, 508-004)
554 was placed on the cured PDMS layer at 8 mm intervals, and another 15 mL PDMS was added to
555 obtain a ~4 mm thick PDMS slab with channels contained inside. Holes crossing the channels
556 were punched at 8 mm intervals using a 5 mm diameter circular punch (Acuderm Inc., P550). A
557 piece of double-sided silicone-based adhesive tape (Adhesives Research, ARCare 90880) was
558 also punched at 8 mm intervals using a 2.5 mm diameter circular punch (Acuderm Inc., P2550).
559 The PDMS slab and the tape were cut into two-well pieces. BIO-133 film, PDMS chunks and
560 double-sided tape were disinfected in 75% ethanol. After disinfection, the BIO-133 membrane
561 was adhered to PDMS via the double-sided adhesive tape, so that the matching holes became
562 wells for cell culture. After growing cells, tubing (Scientific Commodities Inc., BB31695-PE/2)
563 was inserted into both sides of the channel for introducing chemical flow and another piece of
564 double-sided tape without holes was used to seal the wells. The assembly was flipped over for
565 diSPIM imaging through the BIO-133 membrane.
566
567 *Mitochondrial imaging in the presence of CCCP*

568 U2OS cells were cultured in two 5 mm diameter BIO-133 bottomed wells with ports and
569 transfected with 300-400 ng of mEmerald-Tomm20. Before imaging, the wells were filled with
570 live cell imaging solution (Invitrogen, A14291DJ), flipped over and attached to a 10 cm petri dish
571 with double-sided silicone-based adhesive tape (Adhesives Research, ARCare 90880). For the
572 well containing control cells, tubing was left disconnected from a source. For the well
573 containing cells that experienced chemical perturbation, input tubing was connected to a
574 syringe containing 0.05 mM carbonyl cyanide m-chlorophenyl hydrazine (CCCP, Sigma, C2759).
575 The syringe is higher than the output tube so that drug flow was induced by gravity. We used a
576 valve (McMaster-Carr, 7033T21) placed between the input tube and syringe to control the flow.
577 The valve was closed prior to imaging. For each well, two cells were chosen for imaging. A
578 multi-position acquisition was set in the Micro-manager[69] diSPIM plugin[70] to sequentially image
579 the four cells. Volume acquisition time was 3 s, and 90 volumes were acquired for each cell with
580 60 s intervals between volumes. 10 minutes after the imaging started, the valve was opened
581 and drug flow was induced in ~60 s. Dual-view images were deconvolved with ImageJ plugin
582 DiSPIM Fusion[54], drift corrected (ImageJ plugin Correct 3D Drift,
583 https://imagej.net/Correct_3D_Drift) and bleach corrected (ImageJ function Bleach Correction,
584 https://imagej.net/Bleach_Correction, exponential fitting method).
585
586 *Encapsulation of C. elegans into PEG hydrogels*
587 *C. elegans* were encapsulated into PEG hydrogel disks as described in our prior work[7]. PEG
588 hydrogel precursor solutions were prepared by combining 20% w/v poly(ethylene glycol)
589 diacrylate (PEG-DA, 3350 MW, 94.45% acrylation, ESI BIO) with 0.10% w/v Irgacure 2959
590 photoinitiator (2-hydroxy-4'-(2-hydroxyethoxy)-2-methylpropiophenone, I2959, BASF) in 1x S-
591 basal buffer (100 mM NaCl, 50 mM KPO_4 buffer, pH 6.0). Clean 24 mm x 50 mm glass coverslips
592 (VWR) were rendered permanently hydrophobic by exposure to vapors of (tridecafluoro-
593 1,1,2,2-tetrahydrooctyl) trichlorosilane (Gelest). For covalent attachment of the PEG hydrogel
594 to glass, coverslips (Thermo Scientific) were silanized by coating with 3-(trimethoxysilyl)propyl
595 methacrylate (TMSPMA, Sigma-Aldrich). Both methods of surface modification were applied to
596 1" x 3" glass slides (VWR). A small volume (1.75 µL) of PEG hydrogel solution with photoinitiator
597 was pipetted onto a hydrophobic glass slide flanked by two PDMS spacers whose thickness
598 matched the desired hydrogel thickness of 150 µm. Animals were transferred into the hydrogel
599 solution by worm pick. A coverslip, TMSPMA treated for making mounted PEG-DA gels, or
600 untreated for making freestanding gels, was placed over the hydrogel droplet and supported by
601 the PDMS spacers. The glass slide/coverslip sandwich was then placed over a UV light source
602 (312 nm, International Biotechnologies, Inc, model UVH, 12W) and illuminated for two minutes
603 until gelation. Hydrogel disks were immediately transferred to wet agar dishes to keep
604 embedded animals hydrated.
605
606 *Fabrication of microfluidic devices for chemical stimulation of C. elegans*
607 Microfluidic chambers were prepared using poly(dimethyl siloxane) (PDMS; Sylgard 184, Dow
608 Corning) in a ratio of 1:10 and poured to a depth of 5 mm on a silicon master positive mold of
609 the microchannels used previously[71]. Once cut free of the master, devices were punched so
610 that two balanced-length inlets and the outlet had 1.5 mm holes going through the thickness of
611 the material, and 1 mm holes punched from the side to allow flexible tubing to be inserted from

612 the sides. The smooth PDMS device surface opposite the microchannels was irreversibly
613 bonded to a glass slide using oxygen plasma (Harrick PDC-32G, 18W, 45 seconds). A thin PDMS
614 membrane (150 μm) was cut with a 3.5 mm diameter dermal punch and then oxygen plasma
615 bonded to the microfluidic channel surface with the hole in the membrane exposing the
616 micropost array. The hole in the thin PDMS membrane formed a "well" that hydrogel disks
617 could be gently placed in with forceps. A thin BIO-133 membrane (75-80 μm) was prepared by
618 gelation of BIO-133 liquid polymer between two glass slides rendered permanently
619 hydrophobic as described above. Two layers of clear cellophane tape (height of ~80 μm)
620 formed the standoffs that determined final membrane height. After degassing the microfluidic
621 device in a vacuum chamber for approximately 45 minutes, the device was removed from the
622 desiccator, connected to tubing, and flushed with S. basal buffer before use to remove any air
623 bubbles. Hydrogel disks could be interchanged between the well formed by the PDMS above
624 the micropost array easily using forceps and then the system sealed for microfluidic flow using
625 the thin BIO-133 membrane described above. See also **Supplementary Fig. 12**.
626
627 *Preparation of Chemosensory Stimulus*
628 For both wide-field and diSPIM assays, diacetyl (2,3-butanedione, Sigma) was diluted to 1.1 μM
629 in 1x S. basal (10^{-7} dilution). 1 μL of 1 mg/mL fluorescein solution was added to 40 mL of
630 diacetyl solution to visualize stimulus delivery.
631
632 *Wide-field Imaging with Chemical Stimulation*
633 For wide-field, single plane imaging of multiple *C. elegans* at once[57], the microfluidic chamber,
634 valves, tubing and reservoirs were prepared as above and placed on a Zeiss AxioObserver
635 epifluorescence microscope with a 5x, 0.25 NA objective, EGFP filter set, and Hamamatsu Orca-
636 Flash 4 sCMOS camera. Micromanager scripts[72] automatically synchronized capture of ten 30-s
637 trials recording at 10 fps with 10 ms excitation pulses and 10 s chemical stimulation.
638 NeuroTracker software[71] analyzed the wide-field neural imaging data, from which background-
639 corrected fluorescence changes were calculated in MATLAB as $\Delta F/F_0$, where F_0 is baseline
640 neural fluorescence during the four seconds prior to stimulation. Data for multiple individual
641 animals were also presented as a population mean to show the relative decrease in average
642 calcium response after multiple stimulation periods.
643
644 *DiSPIM Imaging with Optical and Chemical Stimulation*
645 Stimulus control for optical illumination or chemical pulses was integrated with diSPIM
646 volumetric imaging using a custom Micromanager script controlling an Arduino Uno and
647 enabling independent digital switching of 6 TTL channels at the beginning of specified image
648 acquisition timepoints. One TTL channel controlled the intensity of a red LED (617 nm, 3W,
649 Mightex) connected to the bottom port of the diSPIM and illuminated the sample through a
650 Nikon 4x, 0.1 NA lower objective. A second TTL channel controlled a 12V fluidic valve system for
651 chemical stimulation (ValveLink 8.2, Automate). Pinch valves allowed flow of either buffer or
652 chemical stimulus lines into the microfluidic channel network, flowing to a common outlet.
653
654 For optogenetic stimulation experiments, animals were embedded in BIO-133 disks bonded to a
655 cover glass placed in the diSPIM sample chamber. To embed animals, they were first transiently

656 immobilized by being picked onto seeded (OP50 *E. coli*) plates with 1 mM tetramisole, and
657 allowed to rest for 1.5 hours. Subsequently, worms were picked into a droplet of BIO-133
658 polymer liquid and gelled in the same manner as the PEG-DA hydrogel disks above, using a
659 TMSPMA silanized coverslip for covalent bonding.
660
661 For chemical stimulation experiments, animals were embedded in PEG hydrogel disks. Animals
662 can be maintained in these disks for many hours if they are kept hydrated[7]. Just prior to an
663 experiment, an animal-embedded disk was inserted into the sample cavity of the diSPIM
664 microfluidic chamber. A 75-80 μm thick BIO-133 membrane was sealed to the microfluidic
665 device surface, closing the fluidic channel with the PEG disk and animals contained within. The
666 hydrogel disk was inserted into a droplet of S. basal buffer present in the well to avoid the
667 introduction of bubbles that would disrupt microfluidic flow. To assure continuous microfluidic
668 flow through the chamber without leaking, we balanced inlet and outlet flows by adjusting the
669 reservoir heights. Specifically, inlet reservoir heights were held slightly above the stage (Δh_{in}),
670 and the outlet reservoir level was placed further below the stage ($\Delta h_{out} > \Delta h_{in}$) to ensure a slight
671 negative pressure in the chamber. Microfluidic stimulus switching was achieved using a dual
672 pinch valve (NResearch Inc., 161P091), that alternately allows either a buffer or stimulus line to
673 flow through the microfluidic chamber to the single outflow line.
674
675 A typical diSPIM acquisition captured one volume per second (10 ms exposure, minimum slice
676 time setting, 55 slices per volume, 166.4 x 166.4 x 82.5 μm total volume space) for 10 minutes,
677 with 20-s duration stimulation every minute. Z-Projection time series videos were produced in
678 ImageJ from cropped versions of the total number of images, then analyzed for GCaMP neural
679 fluorescence using rectangular boxes for integrated fluorescence density, with a nearby region
680 void of signal used for background subtraction.
681
682

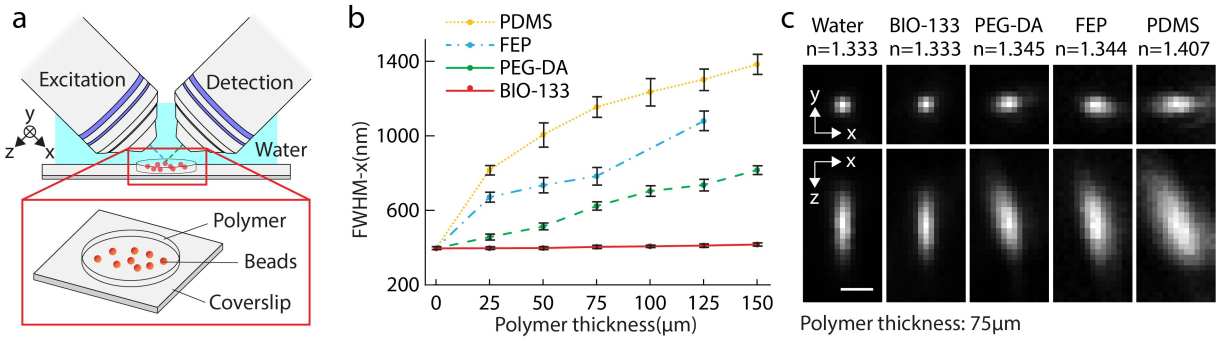

Fig. 1, **Diffraction-limited imaging is possible when imaging through BIO-133, unlike other polymers. a)** Imaging geometry. A light sheet is used to illuminate the 100 nm yellow-green bead sample, which is embedded under progressively thicker polymer. Illumination and detection occur through 0.8 NA water-dipping objectives. **b)** Full width at half maximum (FWHM) in the 'x' direction under different thicknesses of polymer. Means and standard deviations are shown. **c)** Exemplary lateral (top row) and axial (bottom row) images of beads imaged through 75 μm of polymer, demonstrating that BIO-133 provides diffraction-limited performance whilst the other polymers do not. Single images, rather than maximum intensity projections, are shown. The refractive index of each polymer as measured with a refractometer is also indicated (average value from 3 independent trials). Scale bar: 1 μm. See also **Supplementary Table 1**.

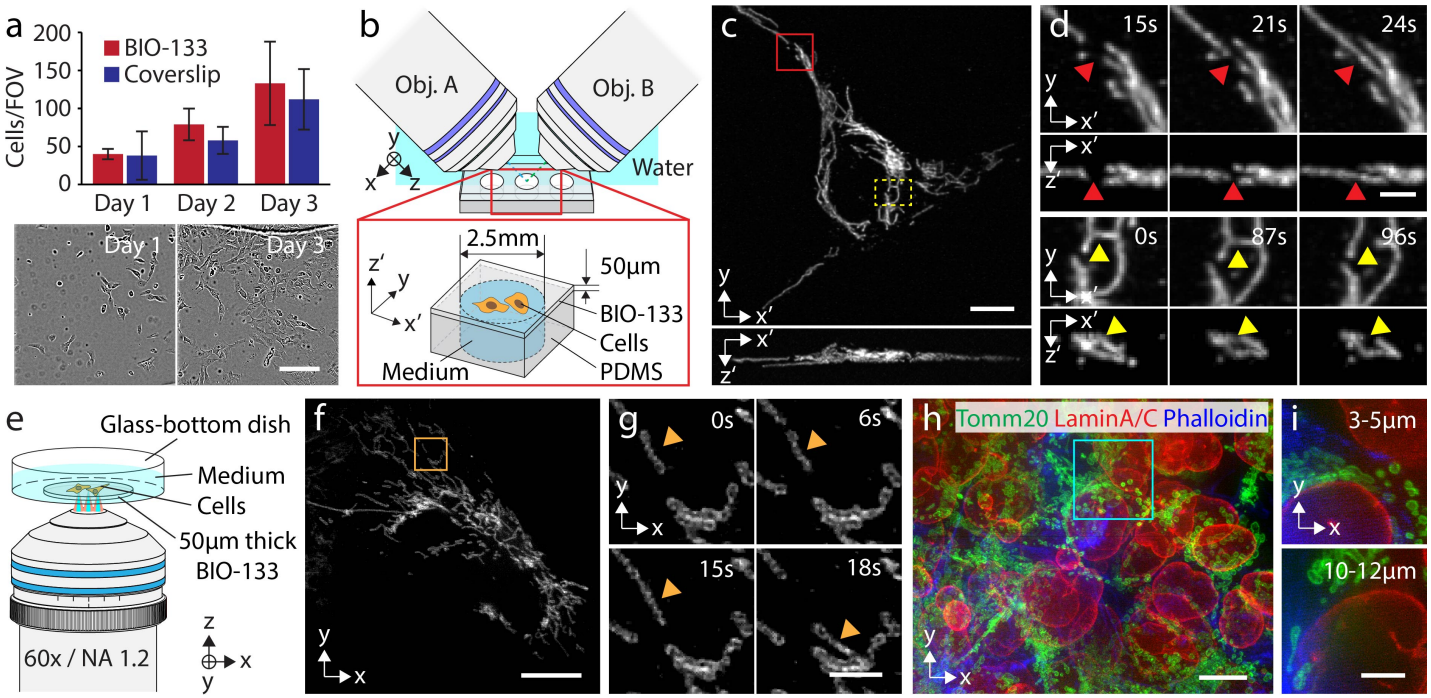

Fig. 2, BIO-133 provides an inert and biocompatible scaffold on which to grow and image cells. **a)** U2OS growth on BIO-133 is similar to growth on glass coverslips. *Top*: quantifying cell growth on 50 µm thick BIO-133 layer vs. glass coverslip. Means and standard deviations from 3 fields of view (10x magnification, ~800 µm x 800 µm field of view) are shown over 3 days. *Bottom*: example fields of view from day 1 and day 3, cells on BIO-133 layer. Scale bar: 200 µm. See also **Supplementary Fig. 2, 3**. **b)** Schematic of diSPIM imaging geometry. 50 µm film with adherent cells is inverted and imaged in the diSPIM setup. See also **Supplementary Fig. 4**. **c**) Example maximum intensity projections of deconvolved images of U2OS cells expressing mEmerald-Tomm20 in lateral (top) and axial (bottom) views. Scale bar: 10 µm. **d)**. Higher magnification views of the red and yellow rectangles in **c)**, highlighting examples of mitochondrial fusion (top, red arrowhead) and fission (bottom, yellow arrowhead). 50 volumes were taken with a 3 s inter-volume interval. See also **Supplementary Video 1**. Note that primed coordinates refer to the plane of the BIO-133 layer (x', y) and the direction normal to the BIO-133 layer (z'). Scale bar: 2 µm. **e**) iSIM imaging geometry. Cells were cultured on 50 µm BIO-133 film, and the film placed in a glass-bottom dish and immersed in cell culture medium. Imaging was performed with a 60x, NA 1.2 water-immersion lens. **f**) Example deconvolved iSIM maximum intensity projection showing live U2OS cells expressing mEmerald-Tomm20. Scale bar: 10 µm. **g)** Higher magnification view of orange rectangular region in **f)**. Orange arrowhead marks the same mitochondrion. 25 volumes were acquired with a 3 s inter-volume interval. See also **Supplementary Videos, 3, 4**. Scale bar: 2 µm. A 0.5 pixel median filter was used to denoise images in **f, g)** prior to display. **h)** Multiple layers of HCT-116 cells were grown on 50 µm BIO-133 layer and immunostained against Tomm20 (green), lamin A/C (red), and actin (blue). See also **Supplementary Video 5.** Scale bar: 10 µm. **i)** Maximum intensity projection over indicated axial range (measured from the bottom of the cell layer) for cyan rectangular region in **h)**. Scale bar: 5 µm.

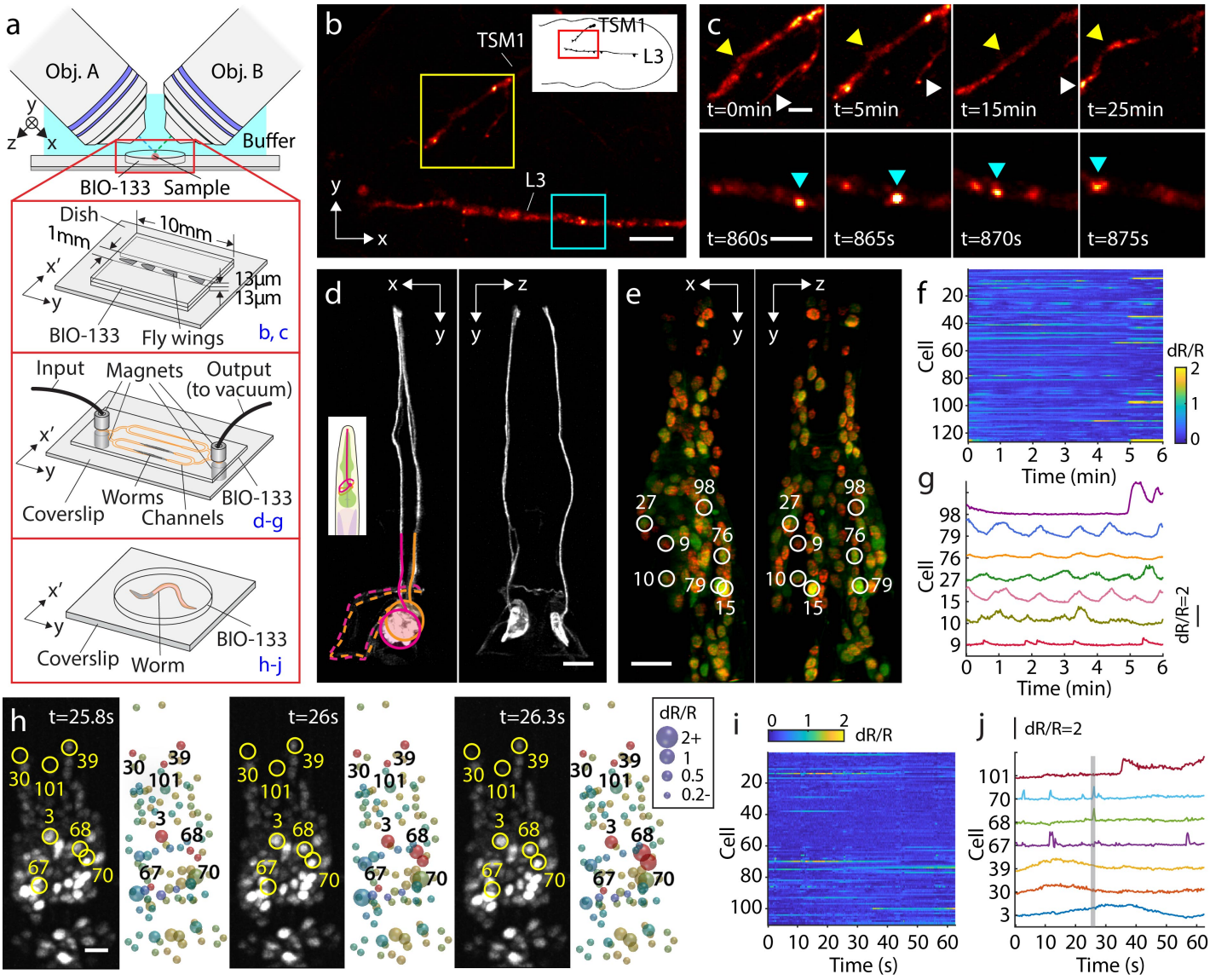

Fig. 3 Live imaging of BIO-133 encapsulated fly wings and *C. elegans*. a) Experimental schematic. Top: A thin layer of BIO-133 membrane covers excised fly wings, immobilizing them so that axon dynamics can be recorded at high resolution over an extended period. Middle: A simple microfluidic device is used to trap adult worms for structural and functional imaging of the nervous system. Bottom: Worms can also be encapsulated in a gelled droplet of BIO-133. See also **Supplementary Figs. 8, 10. b)** Deconvolved, single-view maximum intensity projection of a fly wing with TdTomato-labelled CD4 showing the axons of two neurons (upper: TSM1; lower: L3) shortly before fasciculation in the developing *Drosophila melanogaster* wing disc. Scale bar: 10 µm. 360 volumes were taken with 5 s inter-volume intervals. (30 min in total, see also **Supplementary Video 6**). **c)** Magnified regions of TSM1 and L3 axons, corresponding to yellow and blue rectangles in **b)**, highlighting morphological changes and apparent motion of CD4 puncta. Scale bars: 4 µm. **d)** Isotropic, high-resolution imaging of GFP-labeled axons and dendrites in anesthetized adult *C. elegans*, as shown by orthogonal, jointly deconvolved diSPIM maximum intensity projections. Cell bodies are circled and axons entering the nerve ring region

740 are overlaid with dotted lines. Scale bar: 10 μm. **e)** Calcium imaging of adult worm (red channel:
741 TagRFP, green channel: GCaMP6s; both labels targeted to nuclei), 2 views imaged at 1.25 Hz
742 volumetric rate. Joint deconvolution diSPIM results are shown; red and green channels were
743 simultaneously collected and colors are overlaid in display. Scalebar: 10 μm. See also
744 **Supplementary Video 7. f)** dR/R traces for all 126 tracked nuclei. **g)** dR/R traces for selected
745 individual neurons. Note correspondence with numbered neurons and marked neurons in **e). h)**
746 Calcium imaging of larval worm with higher temporal resolution (4 Hz volumetric rate), single-
747 view results are shown. GCaMP channel and associated segmented dR/R signal are indicated for
748 3 successive time points. Scale bar: 5 μm. See also **Supplementary Video 8. i)** dR/R traces for all
749 110 nuclei segmented and tracked in **h). j)** traces for selected individual neurons. Note
750 correspondence with numbered neurons and marked neurons in **h)**.
751
752

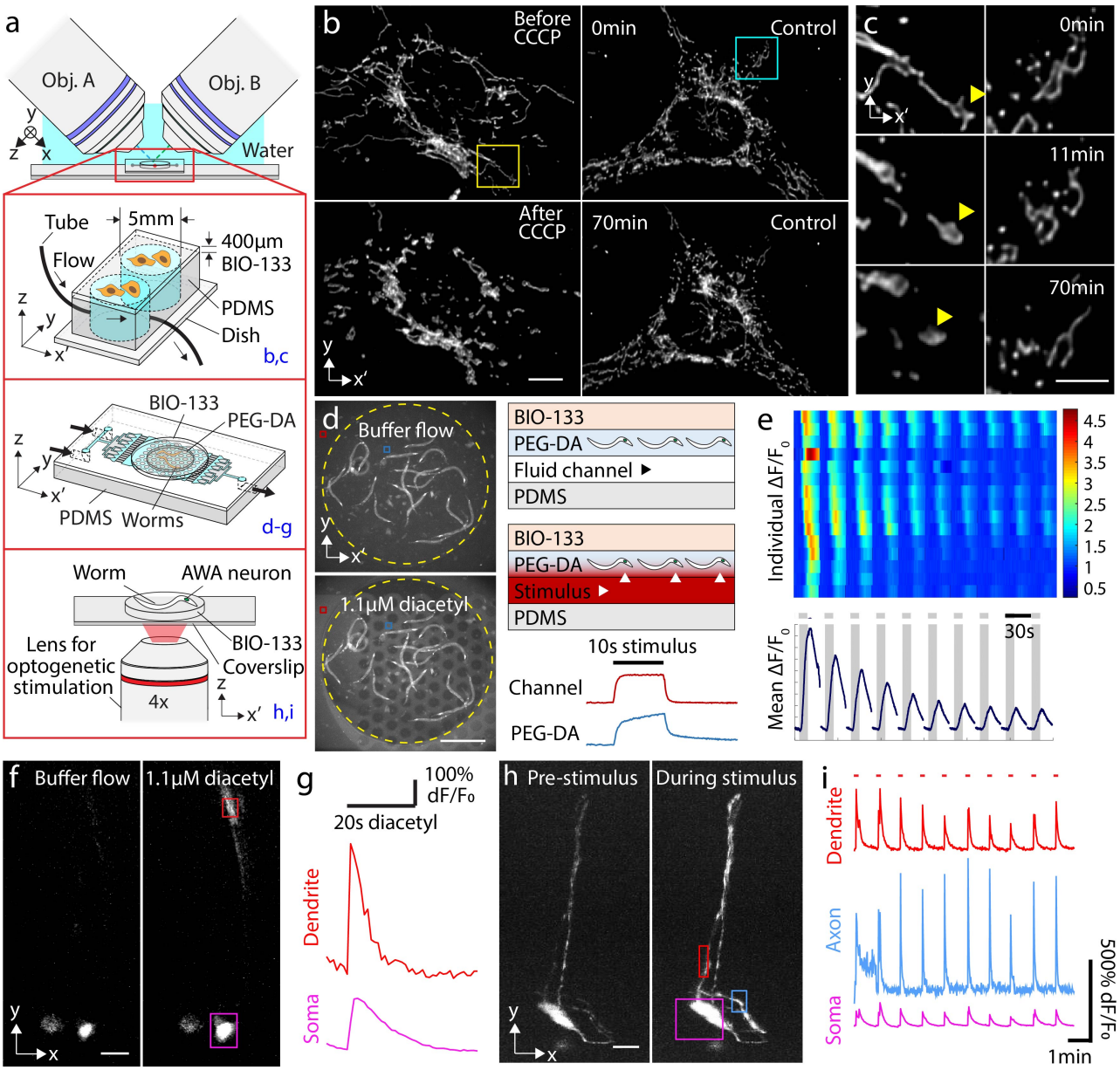

Fig. 4, BIO-133 is compatible with chemical and optical perturbations. a) Experimental schematic for perturbations. Cells grown on BIO-133 were placed on PDMS wells and were either perturbed by flowing 0.05 mM CCCP or left as controls (top higher magnification view). Alternatively, worms were embedded in PEG-DA bonded to a PDMS flow chip and imaged through a layer of BIO-133 (middle higher magnification view) to examine response to chemical stimulation; or embedded in BIO-133, repetitively stimulated with red light from lower, 4x objective and imaged using upper diSPIM objectives (bottom higher magnification view). See also **Supplementary Figs. 11-13**. **b)** Example cells with (left column) and without (right column) CCCP treatment at early (top, 0 min) and late (bottom, 70 min) time points. CCCP was added at 10 minutes. Maximum intensity projections of deconvolved diSPIM data are shown. Scale bar: 10 µm. See also **Supplementary Video 9**. **c)** Higher magnification views of yellow (left column) and blue (right column) regions in **b)**. Yellow arrowhead shows CCCP-induced morphological

766 change of mitochondrion. Scale bar: 5 μm. **d)** Example images of worms expressing GCaMP
767 immobilized in PEG-DA disk with (bottom) and without (top) 1.1 μM diacetyl. Fluorescein added
768 to stimulus highlights the rapid addition/removal of chemical. Scale bar: 500 μm. Right
769 schematics show layered structure of assembly, including direction of flow and diffusion
770 (arrowheads) into PEG-DA layer. Line plots show intensity of fluorescein over time in channel
771 (red) and PEG-DA (blue) layers. **e)** Top: dF/F heatmaps derived from widefield microscopy
772 measurements from 15 animals (rows) in response to 10 repeated stimulus pulses (once per
773 minute). Bottom: responses averaged over all animals show neural adaptation. **f**) Single-view
774 diSPIM images recorded from a single animal, showing subcellular response in AWA neuron to
775 1.1 μM diacetyl compared to control (buffer flow) conditions. Contrast has been adjusted to
776 better highlight the response from different cell regions. Scale bar: 10 μm. See also
777 **Supplementary Video 10**. **g)** Graphs show average intensity from boxed regions in **f)**
778 highlighting fluorescence intensity changes in soma and dendrite. **h)** Worms expressing
779 Chrimson and GCaMP are repetitively stimulated with red light and imaged using upper diSPIM
780 objectives. Maximum intensity projection of GCaMP fluorescence from single-view diSPIM
781 recordings are shown before (left) and after (right) optogenetic stimulation. Scale bar: 10 μm.
782 See also **Supplementary Video 11**. **i)** dF/F traces for dendrite, axon, and soma, corresponding to
783 boxed regions in **h)**.
784

785 **References**

786 1 Chalfie, M., Tu, Y., Euskirchen, G., Ward, W. W. & Prasher, D. C. Green fluorescent
787 protein as a marker for gene expression. *Science* **263**, 802-805 (1994).
788 2 Ou, G., Stuurman, N., D'Ambrosio, M. & Vale, R. D. Polarized Myosin Produces Unequal-
789 Size Daughters During Asymmetric Cell Division. *Science* **330**, 677-680 (2010).
790 3 Kato, S. *et al.* Global brain dynamics embed the motor command sequence of
791 Caenorhabditis elegans. *Cell* **163**, 656-669 (2015).
792 4 Chokshi, T. V., Ben-Yakar, A. & Chronis, N. CO2 and compressive immobilization of C.
793 elegans on-chip. *Lab Chip* **9**, 151-157 (2009).
794 5 Snow, J. J. *et al.* Two anterograde intraflagellar transport motors cooperate to build
795 sensory cilia on *C. elegans* neurons. *Nature Cell Biology* **6**, 1109-1113 (2004).
796 6 Kim, E., Sun, L., Gabel, C. V. & Fang-Yen, C. Long-Term Imaging of Caenorhabditis
797 elegans Using Nanoparticle-Mediated Immobilization. *PLoS One*, e53419 (2013).
798 7 Burnett, K., Edsinger, E. & Albrecht, D. R. Rapid and gentle hydrogel encapsulation of
799 living organisms enables long-term microscopy over multiple hours. *Communications*
800 *biology* **1**, 73 (2018).
801 8 Rohde, C. B., Zeng, F., Gonzalez-Rubio, R., Angel, M. & Yanik, M. F. Microfluidic system
802 for on-chip high-throughput whole-animal sorting and screening at subcellular
803 resolution. *Proc Natl Acad Sci U S A* **104**, 13891-13895 (2007).
804 9 Cornaglia, M., Lehnert, T. & Gijs, M. A. M. Microfluidic systems for high-throughput and
805 high-content screening using the nematode Caenorhabditis elegans. *Lab Chip* **17**, 3736-
806 3759 (2017).
807 10 Berger, S. *et al.* Long-term *C. elegans* immobilization enables high resolution
808 developmental studies in vivo. *Lab Chip* **18**, 1359-1368 (2018).
809 11 Mondal, S. *et al.* Large-scale microfluidics providing high-resolution and high-throughput
810 screening of Caenorhabditis elegans poly-glutamine aggregation model. *Nat Commun.* **7**,
811 13023 (2016).
812 12 Levario, T. J., Zhan, M., Lim, B., Shvartsman, S. Y. & Lu, H. Microfluidic trap array for
813 massively parallel imaging of Drosophila embryos. *Nat Protoc.* **8**, 721-736 (2013).
814 13 Yanik, M. F., Rohde, C. B. & Pardo-Martin, C. Technologies for micromanipulating,
815 imaging, and phenotyping small invertebrates and vertebrates. *Annu Rev Biomed Eng*
816 **13**, 185-217 (2011).
817 14 Shorr, A. Z., Sönmez, U. M., Minden, J. S. & LeDuc, P. R. High-throughput
818 mechanotransduction in Drosophila embryos with mesofluidics *Lab Chip* **19**, 1141-1152
819 (2019).
820 15 Stavrakis, S., Holzner, G., Choo, J. & DeMello, A. High-throughput microfluidic imaging
821 flow cytometry. *Current Opinion in Biotechnology* **55**, 36-43 (2018).
822 16 Probst, R., Cummins, Z., Ropp, C., Waks, E. & Shapiro, B. Flow Control of Small Objects
823 On-Chip: Manipulating Live Cells, Quantum Dots, and Nano-Wires. *IEEE Control Systems*
824 *Magazine* **32**, 26-53 (2012).
825 17 Riba, J., Schoendube, J., Zimmermann, S., Koltay, P. & Zengerle, R. Single-cell dispensing
826 and 'real-time' cell classification using convolutional neural networks for higher
827 efficiency in single-cell cloning. *Scientific Reports* **10**, 1193 (2020).

18 Anagnostidis, V. *et al.* Deep learning guided image-based droplet sorting for on-demand selection and analysis of single cells and 3D cell cultures *Lab Chip* **20**, 889-900 (2020).

19 Lam, J. *et al.* Adaptation of a Simple Microfluidic Platform for High-Dimensional Quantitative Morphological Analysis of Human Mesenchymal Stromal Cells on Polystyrene-Based Substrates. *SLAS Technol.* **22**, 646-661 (2017).

20 Doolin, M. T. & Stroka, K. M. Integration of Mesenchymal Stem Cells into a Novel Micropillar Confinement Assay. *Tissue Engineering Part C: Methods* **25**, 662-676 (2019).

21 Albrecht, D. R. *et al.* Microfluidics-integrated time-lapse imaging for analysis of cellular dynamics. *Integrative Biology* **2**, 278-287 (2010).

22 Reilly, D. K., Lawler, D. E., Albrecht, D. R. & Srinivasan, J. Using an Adapted Microfluidic Olfactory Chip for the Imaging of Neuronal Activity in Response to Pheromones in Male *C. Elegans* Head Neurons. *JoVE* **127**, e56026 (2017).

23 Yemini, E. *et al.* NeuroPAL: A Neuronal Polychromatic Atlas of Landmarks for Whole-Brain Imaging in *C. elegans*. *bioRxiv*, https://doi.org/10.1101/676312 (2019).

24 Cáceres, I. d.-C., Valmas, N., Hilliard, M. A. & Lu, H. Laterally Orienting *C. elegans* Using Geometry at Microscale for High-Throughput Visual Screens in Neurodegeneration and Neuronal Development Studies. *PLoS One* **7**, e35037 (2012).

25 Albrecht, D. R. & Bargmann, C. I. High-content behavioral analysis of Caenorhabditis elegans in precise spatiotemporal chemical environments. *Nat Methods* **8**, 599-605 (2011).

26 Belfer, S. J. *et al.* Caenorhabditis-in-Drop Array for Monitoring *C. elegans* Quiescent Behavior. *Sleep* **36**, 689-698 (2013).

27 Scholz, M., Lynch, D. J., Lee, K. S., Levine, E. & Biron, D. A scalable method for automatically measuring pharyngeal pumping in *C. elegans*. *Journal of Neuroscience Methods* **274**, 172-178 (2016).

28 Atakan, H. B., Cornaglia, M., Mouchiroud, L., Auwerx, J. & Gijs, M. A. M. Automated high-content phenotyping from the first larval stage till the onset of adulthood of the nematode Caenorhabditis elegans. *Lab Chip* **19**, 120-135 (2018).

29 Hulme, S. E. *et al.* Lifespan-on-a-chip: microfluidic chambers for performing lifelong observations of C. elegans. *Lab Chip* **10**, 589-597 (2010).

30 Hwang, H., Krajniak, J., Matsunaga, Y., Benian, G. M. & Lu, H. On-demand optical immobilization of *Caenorhabditis elegans* for high-resolution imaging and microinjection. *Lab Chip* **14**, 3498-3501 (2014).

31 Krajniak, J. & Lu, H. Long-term high-resolution imaging and culture of *C. elegans* in chip-gel hybrid microfluidic device for developmental studies. *Lab Chip* **10**, 1862-1868 (2010).

32 S., N., Stowers, R., Lou, J., Xia, Y. & Chaudhuri, O. Varying PEG density to control stress relaxation in alginate-PEG hydrogels for 3D cell culture studies *Biomaterials* **200**, 15-24 (2019).

33 Zhang, Z. F., Ma, X., Wang, H. & Ye, F. Influence of polymerization conditions on the refractive index of poly(ethylene glycol) diacrylate (PEGDA) hydrogels. *Applied Physics A* **124**, 283 (2018).

34 Wevers, N. R. *et al.* High-throughput compound evaluation on 3D networks of neurons and glia in a microfluidic platform. *Scientific Reports* **6**, 38856 (2016).

871 35 Pittman, W. E., Sinha, D. B., Zhang, W. B., Kinser, H. E. & Pincus, Z. A simple culture
872 system for long-term imaging of individual *C. elegans*. *Lab Chip* **17**, 3909-3920 (2017).
873 36 Kim, D. N. H., Kim, K. T., Kim, C., Teitell, M. A. & Zangle, T. A. Soft lithography fabrication
874 of index-matched microfluidic devices for reducing artifacts in fluorescence and
875 quantitative phase imaging. *Microfluidics and Nanofluidics* **22** (2017).
876 37 Polanco, E. R., Western, N. & Zangle, T. A. Fabrication of Refractive-index-matched
877 Devices for Biomedical Microfluidics. *J Vis Exp* **139**, 58296 (2018).
878 38 Levario, T. J., Insley, P., Hwang, H., Shaham, S. & Lu, H. in *18th International Conference*
879 *on Miniaturized Systems for Chemistry and Life Sciences, MicroTAS 2014* 727-729 (San
880 Antonio, TX, 2014).
881 39 Xu, T. *et al.* Modified inverted selective plane illumination microscopy for
882 submicrometer imaging resolution in polydimethylsiloxane soft lithography devices. *Lab*
883 *Chip* **Advance Online Publication**, doi:https://doi.org/10.1039/D0LC00598C (2020).
884 40 Chang, T.-Y., Pardo-Martin, C., Allalou, A., Wählby, C. & Yanik, M. F. Fully automated
885 cellular-resolution vertebrate screening platform with parallel animal processing. *Lab*
886 *Chip* **12**, 711-716 (2012).
887 41 Tonin, M., Descharmes, N. & Houdré, R. Hybrid PDMS/glass microfluidics for high
888 resolution imaging and application to sub-wavelength particle trapping. *Lab Chip* **16**,
889 465-470 (2016).
890 42 Turaga, D. & Holy, T. E. Miniaturization adn defocus correction for objective-coupled
891 planar illumination microscopy. *Optics Letters* **33**, 2302-2304 (2008).
892 43 Wu, Y. *et al.* Spatially isotropic four-dimensional imaging with dual-view plane
893 illumination microscopy. *Nat Biotechnol.* **31**, 1032-1038 (2013).
894 44 Chen, B. C. *et al.* Lattice light-sheet microscopy: imaging molecules to embryos at high
895 spatiotemporal resolution. *Science* **346**, 1257998 (2014).
896 45 Hedde, P. N., Malacrida, L., Ahrar, S., Siryaporn, A. & Gratton, E. sideSPIM - selective
897 plane illumination based on a conventional inverted microscope. *Biomedical Optics*
898 *Express* **8**, 3918-3937 (2017).
899 46 Kumar, A. *et al.* Dual-view plane illumination microscopy for rapid and spatially isotropic
900 imaging. *Nature Protocols* **9**, 2555-2573 (2014).
901 47 Kaufmann, A., Mickoleit, M., Weber, M. & Huisken, J. Multilayer mounting enables long-
902 term imaging of zebrafish development in a light sheet microscope. *Development* **139**,
903 3242-3247 (2012).
904 48 York, A. G. *et al.* Instant super-resolution imaging in live cells and embryos via analog
905 image processing. *Nat Methods* **10**, 1122-1126 (2013).
906 49 Murray, M. A., Schubiger, M. & Palka, J. Neuron Differentiation and Axon Growth in the
907 Developing Wing of *Drosophila melanogaster*. *Developmental Biology* **104**, 259-273
908 (1984).
909 50 Jan, Y. N., Ghysen, A., Christoph, I., Barbel, S. & Jan, L. Y. Formation of Neuronal
910 Pathways in the Imaginal Discs of *Drosophila melanogaster*. *The Journal of Neuroscience*
911 **5**, 2453-2464 (1985).
912 51 Clarke, A. *et al.* Dynamic Morphogenesis of a Pioneer Axon in *Drosophila* and Its
913 Regulation by Abl Tyrosine Kinase. *Mol Biol Cell* **31**, 452-465 (2020).

914 52 Clarke, A. *et al.* Abl Signaling Directs Growth of a Pioneer Axon in *Drosophila* by Shaping
915 the Intrinsic Fluctuations of Actin. *Mol Biol Cell* **31**, 466-477 (2020).
916 53 Hulme, S. E., Shevkoplyas, S. S., Apfeld, J., Fontana, W. & Whitesides, G. A
917 Microfabricated Array of Clamps for Immobilizing and Imaging *C. Elegans*. *Lab Chip* **7**,
918 1515-1523 (2007).
919 54 Guo, M. *et al.* Rapid image deconvolution and multiview fusion for optical microscopy.
920 *Nature Biotechnol.*, in press, doi:https://doi.org/10.1038/s41587-020-0560-x (2020).
921 55 Chen, T.-W. *et al.* Ultra-sensitive fluorescent proteins for imaging neuronal activity.
922 *Nature* **499**, 295-300 (2013).
923 56 Nguyen, J. P., Linder, A. N., Plummer, G. S., Shaevitz, J. W. & Leifer, A. M. Automatically
924 tracking neurons in a moving and deforming brain. *PLoS Comput Biol.* **13**, e1005517
925 (2017).
926 57 Larsch, J., Ventimiglia, D., Bargmann, C. I. & Albrecht, D. R. High-throughput imaging of
927 neuronal activity in Caenorhabditis elegans. *PNAS* **110**, E4266-4273 (2013).
928 58 Sengupta, P., Chou, J. H. & Bargmann, C. I. odr-10 Encodes a Seven Transmembrane
929 Domain Olfactory Receptor Required for Responses to the Odorant Diacetyl. *Cell* **84**,
930 899-909 (1996).
931 59 Shidara, H., Hotta, K. & Oka, K. Compartmentalized cGMP Responses of Olfactory
932 Sensory Neurons in *Caenorhabditis elegans*. *Journal of Neuroscience* **37**, 3753-3763
933 (2017).
934 60 Klapoetke, N. C. *et al.* Independent optical excitation of distinct neural populations.
935 *Nature Methods* **11**, 338-346 (2014).
936 61 Martin, C. *et al.* Line excitation array detection fluorescence microscopy at 0.8 million
937 frames per second *Nature Communications* **9**, 4499 (2018).
938 62 Han, Y. *et al.* Cameraless high-throughput three-dimensional imaging flow cytometry.
939 *Optica* **6**, 1297-1304 (2019).
940 63 Ravasio, A., Vaishnavi, S., Ladoux, B. & Viasnoff, V. High-resolution imaging of cellular
941 processes across textured surfaces using an index-matched elastomer. *Acta Biomater.*
942 **14**, 53-60 (2015).
943 64 Xiao, F., Wen, X., Tan, X. H. M. & Chiou, P.-Y. Plasmonic micropillars for precision cell
944 force measurements across a large field-of-view *Appl. Phys. Lett.* **112**, 033701 (2018).
945 65 Duffy, D. C., McDonald, J. C., Schueller, O. J. & Whitesides, G. M. Rapid Prototyping of
946 Microfluidic Systems in Poly(dimethylsiloxane). *Anal Chem* **70**, 4974-4984 (1998).
947 66 Guo, M. *et al.* Single-shot super-resolution total internal reflection fluorescence
948 microscopy. *Nature Methods* **15**, 425-428 (2018).
949 67 Xia, Y. & Whitesides, G. M. Soft Lithography. *Angew. Chem. Int. Ed. Engl.* **37**, 550-575
950 (1998).
951 68 Atencia, J. *et al.* Magnetic connectors for microfluidic applications *Lab Chip* **10**, 246-249
952 (2010).
953 69 Edelstein, A. D. *et al.* Advanced methods of microscope control using μManager
954 software. *Journal of Biological Methods* **1**, e11 (2014).
955 70 Ardiel, E. L. *et al.* Visualizing Calcium Flux in Freely Moving Nematode Embryos. *Biophys.*
956 *J.* **112**, 1975-1983 (2017).

957 71 Lagoy, R. C. & Albrecht, D. R. Microfluidic Devices for Behavioral Analysis, Microscopy,
958 and Neuronal Imaging in Caenorhabditis elegans. *Methods Mol Biol.* **1327**, 159-179
959 (2015).
960 72 Lagoy, R. C. & Albrecht, D. R. Automated fluid delivery from multiwell plates to
961 microfluidic devices for high-throughput experiments and microscopy. *Sci. Reports* **8**,
962 6217 (2018).
963